

## Rock bridge fracture model and stability analysis of surrounding rock in underground cavern group

Song Yu<sup>1,2</sup>, Wei-shen Zhu<sup>\*1,3</sup>, Wei-min Yang<sup>3</sup>, Dun-fu Zhang<sup>2</sup> and Qing-song Ma<sup>3</sup>

<sup>1</sup>State Key Laboratory of Geomechanics and Geotechnical Engineering, Institute of Rock and Soil Mechanics, Chinese Academy of Sciences, Wuhan, 430071, China

<sup>2</sup>School of Civil Engineering, Shandong University, Ji'nan, 250061, China

<sup>3</sup>Geotechnical and Structural Engineering Research Center, Shandong University, Ji'nan, 250061, China

(Received January 29, 2013, Revised May 14, 2014, Accepted October 29, 2014)

**Abstract.** Many hydropower stations in southwest China are located in regions of brittle rock mass with high geo-stresses. Under these conditions deep fractured zones often occur in the sidewalls of the underground caverns of a power station. The theory and methods of fracture and damage mechanics are therefore adopted to study the phenomena. First a flexibility matrix is developed to describe initial geometric imperfections of a jointed rock mass. This model takes into account the area and orientation of the fractured surfaces of multiple joint sets, as well as spacing and density of joints. Using the assumption of the equivalent strain principle, a damage constitutive model is established based on the brittle fracture criterion. In addition the theory of fracture mechanics is applied to analyze the occurrence of secondary cracks during a cavern excavation. The failure criterion, for rock bridge coalescence and the damage evolution equation, has been derived and a new sub-program integrated into the FLAC-3D software. The model has then been applied to the stability analysis of an underground cavern group of a hydropower station in Sichuan province, China. The results of this method are compared with those obtained by using a conventional elasto-plastic model and splitting depth calculated by the splitting failure criterion proposed in a previous study. The results are also compared with the depth of the relaxation and fracture zone in the surrounding rock measured by field monitoring. The distribution of the splitting zone obtained both by the proposed model and by the field monitoring measurements are consistent to the validity of the theory developed herein.

**Keywords:** underground cavern group; splitting failure; damage evolution equation; numerical analysis; field monitoring

### 1. Introduction

In the area of southwest China there are a number of hydropower stations with underground caverns being in designing or construction stage. The structural stability of these underground openings under different site conditions is a vital issue in their engineering, excavation and operation. The rock masses in the vicinity of these power stations have often a complex geologic body with variable initial stress field, and deferent rock mass properties.

---

\*Corresponding author, Professor, E-mail: [zhuw@sdu.edu.cn](mailto:zhuw@sdu.edu.cn)

The rock mass will exhibit various macro geological structure surfaces such as joints, faults, and cracks. Because of these features the deformation and strength characteristics of the rock mass, are to a large extent, controlled by the discontinuous nature of the rock. The research on modeling of crack initiation and propagation of primary joints is important in the understanding of the fracture mechanisms of the rock mass so as to be able to judge the stability of the cavities group. Therefore the numerical simulation of the fracture process of a rock mass has become a considered approach to analyze rock mass behavior and its engineering stability. Yoshida and Horii (2004) and other authors (2005) conducted stability analyses on specific projects using the finite element methods, DDA and the 2D or 3D discrete element methods. Hibino (2003) investigated 16 large-scale underground power stations in Japan and found that for caverns excavated in typical igneous rock, approximately 2/3 of the sidewall deformation could be attributed to cavity displacement of open cracks. Yoshida (2003) presented a continuum model based on micro mechanics. Maghousa (2008) derived an elasto-plastic constitutive model for jointed rock using the homogenization method for randomly heterogeneous medium. Jiang (2009) simulated a crack initiation and the evolution process by applying the EDEM method. Zhu *et al.* (2008) conducted studies on the displacement prediction in high sidewalls for typical opening complexes under different conditions and with various factors which influence the displacements around the caverns. These studies demonstrated the significance of properties such as the rock density and dip angles and positions of discontinuities on the mechanical behavior of the cavity structures and proved the effectiveness of DEM to study these cavity problems in a discontinuous rock mass.

Although there have been many investigations into cavern stability by numerical or in situ monitoring, comprehensive, systematic studies on stability of large multiple openings under different conditions have rarely been reported. In this paper, a damage evolution constitutive model for a rock mass is presented by integrated macroscopic damage mechanics and microscopic fracture mechanics. The mechanism of secondary cracks and rock bridge coalescence are studied and from this a damage evolution equation and constitutive model for a rock mass is obtained. The subroutine with this model is then interfaced with the commercial FLAD-3D software. The method is then applied to stability analysis of an underground cavern group. And the results are compared with the field monitoring data for comparison and calibration.

## 2. Algorithm for subroutine to include rock fracture used with FLAC-3D

### 2.1 Modified constitutive equation for jointed rock mass

The constitutive equation for general rock masses without joints or cracks can be expressed as following

$$[\varepsilon] = [C^0][\sigma] \quad (1)$$

Where the  $[C^0]$  is flexibility matrix for rock, it can be written

$$[C^0] = \begin{bmatrix} C_{11}^0 & C_{12}^0 & 0 \\ C_{21}^0 & C_{22}^0 & 0 \\ 0 & 0 & C_{33}^0 \end{bmatrix} \quad (2)$$

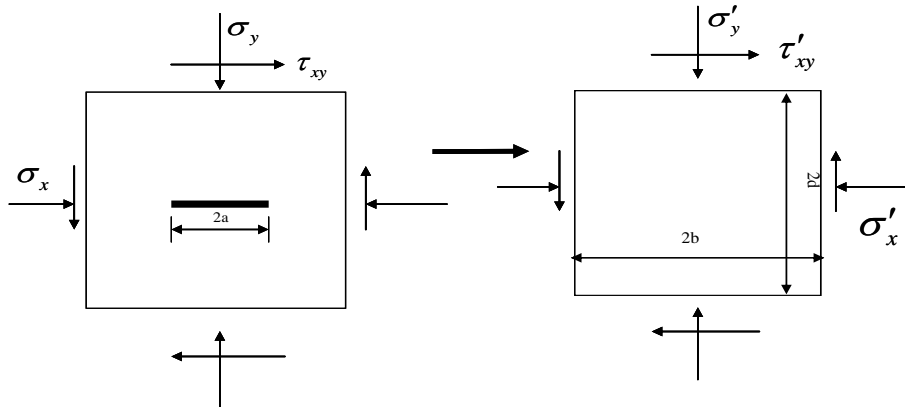


Fig. 1 Equivalence of fractured rock mass

However the constitutive equation for the jointed rock mass differs from the above when joints and cracks are present. The stress status for jointed rock is assumed equivalent to that in the intact rock, as shown in Fig. 1.

In Fig. 1,  $a$ ,  $b$  and  $c$  are defined,  $a$  is the half of length of a crack,  $2b$  and  $2d$  are the equivalent breadth length and thickness respectively of rock element containing the crack. The presence of cracks results in a reduction in stiffness of the altered rock from that of the intact rock. The flexibility matrix has the following form

$$[C] = \begin{bmatrix} C_{11} & C_{12} & 0 \\ C_{21} & C_{22} & 0 \\ 0 & 0 & C_{33} \end{bmatrix} \quad (3)$$

It is assumed that a joint or crack has no affected on Poisson's ratio of rock mass, so that:

$$C_{11} = E_0^{-1} \quad (4)$$

$$C_{12} = C_{21} = -\nu_0 / E_0 \quad (5)$$

$E_0$  and  $\nu_0$  are the Young's modulus and Poisson's ratio for the rock element, and assuming that joints or cracks have no effect on Poisson's ratio. Based on the energy reciprocity principle, the following equations can be obtained

$$C_{22} = C_{22}^0 + \frac{aC_n}{K_n \cdot 2bd} \quad (6)$$

$$C_{33} = C_{33}^0 + \frac{aC_s}{K_s \cdot 2bd} \quad (7)$$

Let normal compressive transferable coefficient of cracks be  $C_n$ ,  $C_s$  for shear transformed coefficient,  $K_n$  for normal stiffness, and  $K_s$  for shear stiffness in Kawamoto's model (1988).  $C_n$  and  $C_s$  in the above Eqs. (6) and (7) can be determined according to Kunin (1983)

$$C_n = \frac{\pi a}{\pi a + \frac{E_0}{1-\nu_0^2} \cdot \frac{1}{K_n}} \quad (8)$$

$$C_s = \frac{\pi a}{\pi a + \frac{E_0}{1-\nu_0^2} \cdot \frac{1}{K_s}} \quad (9)$$

When  $n$  groups of arbitrarily oriented cracks are distributed in the rock mass, it is assumed that the flexibility matrix can be obtained by superposition of the separate values

$$[C] = [C^0] + \sum_{i=1}^n [A_i^{-1}]^T [\Delta C_i] [A_i]^{-1} \quad (10)$$

For two-dimensional case, the Eq. (10) can be also written as

$$[C^0] = \begin{bmatrix} \frac{1}{E_0} & -\frac{\nu_0}{E_0} & 0 \\ -\frac{\nu_0}{E_0} & \frac{1}{E_0} & 0 \\ 0 & 0 & \frac{1}{G} \end{bmatrix} \quad (11)$$

Where:  $[A_i]$  coordinate transformation matrix

$$[A_i] = \begin{bmatrix} \cos^2 \alpha_i & \sin^2 \alpha_i & -\sin 2\alpha_i \\ \sin^2 \alpha_i & \cos^2 \alpha_i & \sin 2\alpha_i \\ \frac{1}{2} \sin 2\alpha_i & -\frac{1}{2} \sin 2\alpha_i & \cos 2\alpha_i \end{bmatrix} \quad (12)$$

$\alpha_i$  is the angle between global and local coordinate system,  $[\Delta C_i]$  ith flexibility increment matrix

$$[\Delta C_i] = \begin{bmatrix} 0 & 0 & 0 \\ 0 & \frac{C_n^i a}{K_n^i 2b_i d_i} & 0 \\ 0 & 0 & \frac{C_s^i a}{K_s^i 2b_i d_i} \end{bmatrix} \quad (13)$$

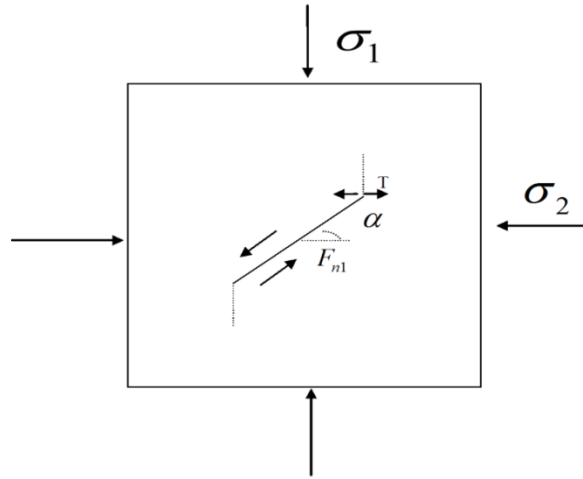


Fig. 2 Original and secondary cracks in rock mass

### 2.2 Formation of secondary wing cracks

It is assumed that a sample with an initial crack inside is loaded by the stresses  $\sigma_1$  and  $\sigma_2$  in vertical and horizontal directions respectively and the secondary cracks develop along the direction of the major principal stress. These cracks are controlled mainly by the crack surface force  $F_{n1}$  and tension force  $T$  which is perpendicular to the secondary crack surface. The secondary cracks can be equivalent to two cracks parallel to the major principal stress, as shown in Fig. 2. The  $F_{n1}$  and  $T$  can be calculated

$$F_{n1} = |(\sigma_1 - \sigma_2) \cdot \sin \alpha \cdot \cos \alpha| - f_j \cdot H(\sigma_n) \cdot \sigma_n - c_j \quad (14)$$

$$T = 2aF_{n1} \cos \alpha \quad (15)$$

Where

$$\sigma_n = \sigma_1 \cdot \cos^2 \alpha + \sigma_2 \cdot \sin^2 \alpha \quad (16)$$

$$H(\sigma_n) = \begin{cases} 1 & \sigma_n > 0 \\ 0 & \sigma_n \leq 0 \end{cases} \quad (17)$$

$f_j$  and  $c_j$  are friction coefficient and cohesion of the initial crack surface, respectively.  $\alpha$  is the angle between crack and major principal stress.

If the shear stress on the crack surface is greater than the shear strength, then secondary cracks occur at the tip of the original crack. From Fig. 3, the stress intensity factor at crack tip can be written as

$$K_I = \frac{2.589T}{\sqrt{\pi L}} - 1.12147\sigma_2 \cdot \sqrt{\pi L} \quad (18)$$

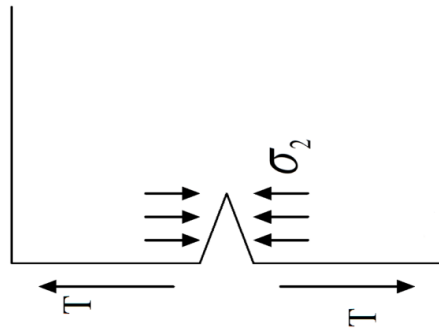


Fig. 3 Sketch of stress field for secondary crack

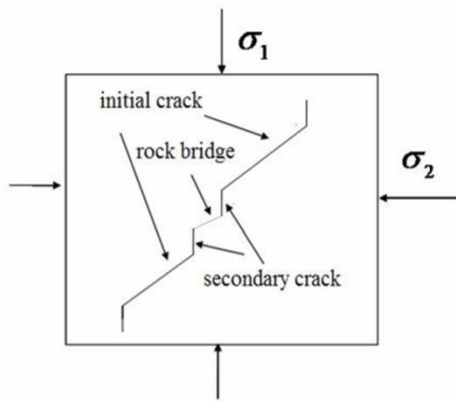


Fig. 4 General failure mode of rock mass with multiple parallel cracks

In case of tension crack model

$$K_I = K_{IC} \tag{19}$$

The secondary crack length is

$$L = \frac{1}{\pi} \left[ \frac{\sqrt{K_{IC}^2 + 11.614T\sigma_2} - K_{IC}}{2.243\sigma_2} \right] \tag{20}$$

For multiple cracks coupling case, the crack interaction factor  $F_I$  is introduced as

$$K'_I = F_I \cdot K_I \tag{21}$$

Substituting into Eq. (20), it follows that

$$L = \frac{1}{\pi \cdot F_I^2} \left[ \frac{\sqrt{K_{IC}^2 + 11.614T\sigma_2} - K_{IC}}{2.243\sigma_2} \right] \tag{22}$$

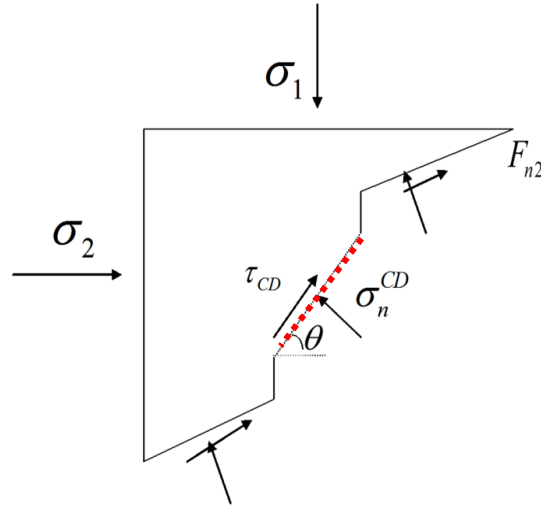


Fig. 5 Shear failure of rock bridge in rock mass with multiple cracks (dashed line indicates rock bridge)

### 2.3 Rock bridge coalescence in rock mass with multiple cracks

In rock mass with multiple parallel cracks, the rock bridge will be formed under two or three-dimensional compression. The failure model with two parallel cracks is shown in Fig. 4.

As the crack surface when shear stress.  $F_{n1} = |(\sigma_1 - \sigma_2) \cdot \sin\alpha \cdot \cos\alpha| - f_j \cdot H(\sigma_n) \cdot \sigma_n - c_j > 0$ , secondary cracks occur. When the secondary crack propagates to some extent, rock bridge coalesces due to shear stress, being greater than shear strength as illustrated in Fig. 8, and leads to the failure of rock mass. In Fig. 5, it is shown that the shear failure is mainly caused by the shear stress  $F_{n2}$ . Stress analysis given as following

$$F_{n2} = \tau^{CD} - f_k \cdot H(\sigma_n^{CD}) \cdot \sigma_n^{CD} - c_k \quad (23)$$

in which

$$H(\sigma_n^{CD}) = \begin{cases} 1 & \sigma_n^{CD} > 0 \\ 0 & \sigma_n^{CD} \leq 0 \end{cases} \quad (24)$$

and

$$\tau^{CD} = \frac{\sigma_1 - \sigma_2}{2} \cdot \sin 2\theta \quad (25)$$

$$\sigma_n^{CD} = \sigma_1 \cdot \cos^2 \theta + \sigma_2 \sin^2 \theta \quad (26)$$

The terms,  $f_k$  and  $c_k$  are friction coefficient and cohesion of rock. When  $F_{n2} = 0$ , the rock bridge fracture will be occur.

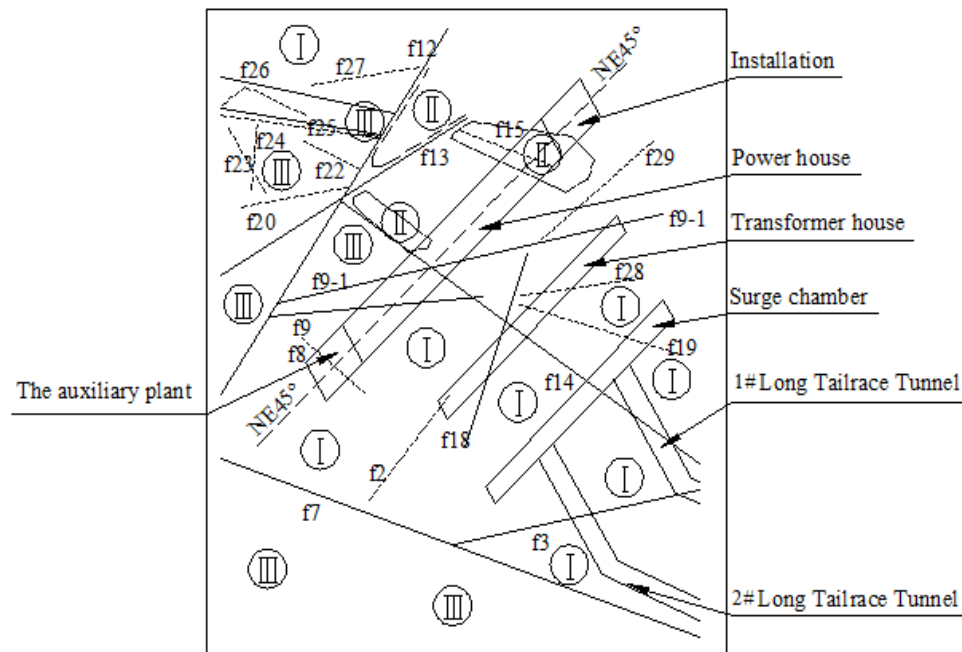


Fig. 6 Rock classification of surrounding rock masses in underground powerhouse zone at elevation 688m

### 3. Engineering application and failure analysis of rock surrounding

In this section the algorithm for the rock mass damage fracture model and fracture evolution equation (discussed in the section 2), is written in a subroutine which is then interfaced with the FLAC-3D analysis program and the model and methods applied to the stability study of an underground cavity complex of a power station excavated in the rock mass.

#### 3.1 Engineering background and geological conditions

Pubugou hydropower station, located on the upper reaches of the Dadu River is one of the largest cascade development stations in China. Underground caverns located downstream on the left bank of dam axis in granite, about 400 m from the shore. The cavern group is composed of main and auxiliary powerhouse, a transformer house, surge chamber, 2 tail water tunnels and 6 diversion tunnels. The main and auxiliary powerhouses, as well the transformer house and the surge chamber are arranged in parallel, the longitudinal axis of the main power house is in the direction N42°E. The main powerhouse and transformer house are 41.95m, apart and the transformer house and surge chamber 32.70m, apart. The depth of the three larger caverns is more than 200 m.

Geostresses of the station area are controlled mainly by the tectonic stresses. The maximum principle stress  $\sigma_1=21.1-27.3\text{MPa}$ , three mean stresses deviation are  $\sigma_1: \sigma_2: \sigma_3=1:0.65:0.27$ , The ratio, uniaxial compressive strength  $\sigma_c$  to maximum principal stress  $\sigma_1$  is 4.4-5.9, and angle between the longitudinal axis of powerhouse and the direction of the maximum principal stress varies  $12^\circ\sim 42^\circ$ .

Table 1 Pysico-mechanical parameters of rock mass

Class of surrounding rock	Rock classification and characteristics	Density $\rho$ (g·cm <sup>-3</sup> )	Modulus of deformation $E_0$ /GPa	Young's modulus $E$ /GPa	Poisson's ratio	Cohesion MPa	$\tan \varphi$
I	Fresh, intact granite	2.66	27-30	35-40	0.18	3.0	1.73
II	Fresh or light weathering blocky granite	2.61	15-20	20-26	0.21	2.0	1.42
II	Fresh or light weathering blocky basalt	3.07	12-18	18-26	0.23	2.6	1.42
III	Weak weathered sub-blocky granite	2.61	8-13	10-17	0.25	1.2	1.10
III	Weak weathered basalt with mosaic structure	2.88	6-10	8-15	0.27	1.5	1.10
IV	Fresh or light weathering tuff with mosaic structure	2.71	3-5	8-15	0.27	0.6	0.84
IV	Weak unloaded zone of granite or basalt	2.5	1-3	4-6	0.3	0.5	0.84
V	Fractured tuff, strong weathering zone, strong unloading zone, fault zone	-	<1	<1	0.35	-	-

Geological information obtained during the excavation showed no large fault crossing the plant area, and the fractures consisted mainly of the III, IV class structures surfaces such as small faults and joints. In the main the direction of longitudinal axis of the powerhouse and the main direction of fracture structure face is greater than 50°.

The rock surrounding of plant caverns is a middle coarse grained granite; uniaxial compressive strength greater than 100 MPa, the physical mechanical parameters of the rocks are given in Table 1. There are three major areas of rock mass quality (see Fig. 6.): The west area away from f12, f13, small faults are developed, rock mass integrity is poor, and it belongs to III class according to the Chinese national classification for rock. In the south region, away from f7, rock is weakly weathered, and is of class III. The east area away from f12, f13 and the north area away from f7, rock mass has a simple, integral structure and of I, II class.

The theoretical model presented in Section 2 is used to study the stability of the surrounding rock of the caverns of Pubugou hydropower station. The main cavern group of the project consists of the powerhouse, the transformer house and surge chamber, see Fig. 7, whose dimensions (width and height) being (27×71 m, 26×33) m and (20×56) m, respectively. The three caverns are parallel in plan. The computation domain covers 540m along the X direction and 740m in the Y direction. The quasi-three-dimensional model (103222 nodes, 88886 elements) has a dimension of 32m in the Z direction.

### 3.2 Excavation scheme

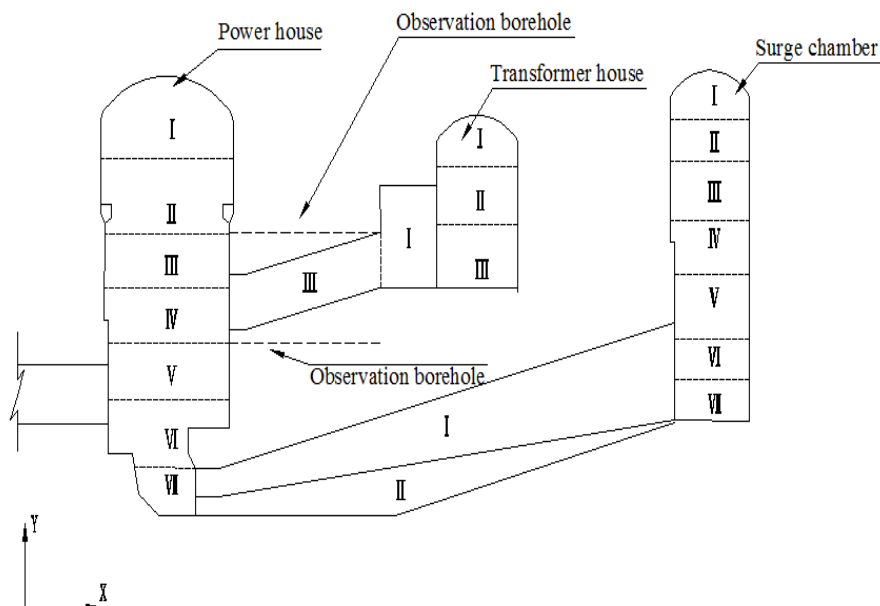


Fig. 7 Sketch of stepwise excavation of underground powerhouse chambers

The caverns, see Fig. 7, were formed by sublevel excavation, in steps from their tops, power house 9, main transformer house 3 and surge chamber 7 steps.

Displacement measuring instruments were installed in several profiles of the underground cavern group. From statistical analysis of the measurement data, the convergence displacements for cavern walls are characterized:

- displacements in the range, 10 mm 46.4% ,
- displacements greater than 20 mm 30% ,
- displacements greater than 40 mm 9.6%,
- displacements greater than 50 mm 6% respectively, of the total.

For the power house the displacements of the upstream side wall and top arch are small, larger displacements occur in the downstream side wall and two crane beams, have values of over 20 mm. The maximum displacement of surrounding rock is at downstream crane beam of turbine unit 2# section, with the final accumulated displacement being approximately 80mm.

For the transformer house the largest displacements occur in its upstream side wall, the upstream arch abutment and the downstream side wall locations, with deformations less than 30 mm.

For the surge chamber the maximum deformation of approximately 85 mm occurs in the side wall at unit 2# turbine location.

The locations maximum displacement values in the surge chamber and the position of maximum deformation for transformer house correspondence with one another. Since the F19 passes between the transformer house and surge chamber, and it indicates that Fault F19 is the main geological factor which causes the large deformations of transformer house downstream side wall and surge chamber upstream side wall for the section of turbine unit 2#.

In general, the positions with large deformation of the caverns and the reasons for the deformations are caused by the geological environment and the nearby construction conditions.

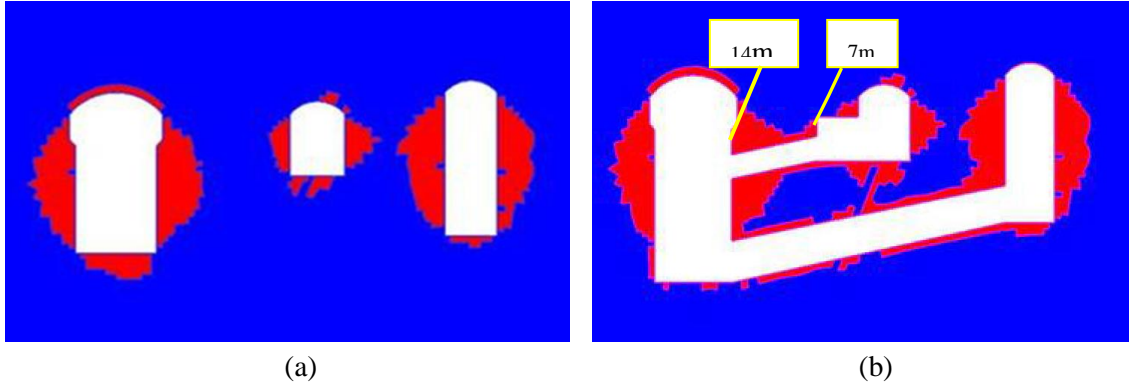


Fig. 8 Cross-sectional view of splitting damage zones (A: Z=1 m) and Cross-sectional view of splitting damage zones (B:Z=15 m)

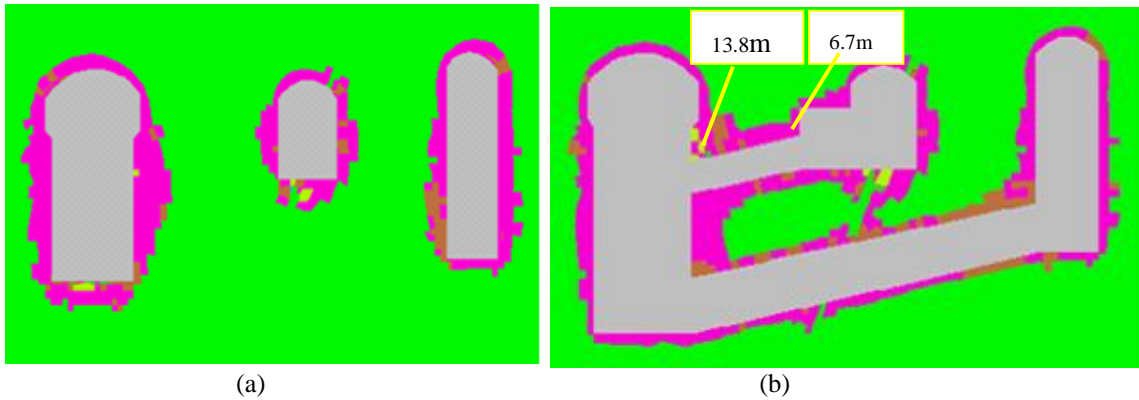


Fig. 9 Cross-sectional view of damage zones (A: Z=1 m) and Cross-sectional view of damage zones (B: Z=15 m)

### 3.3 Simulation result and analysis

From the computation results, the estimated damage evolution zones in the surrounding rock mass are in Fig. 8. Fig. 8(a) shows damage zone (red area) in the cross-section position Z=1 m without connect bridge, and Fig. 8(b) shows damage zone in the cross-section position Z=15 m with connect bridge. In Fig. 8 the depth of the damage evolution zone is estimated to be 14.7 m in the downstream sidewall of the powerhouse and 7 m in the upstream sidewall of the transformer chamber.

A splitting failure criterion for the surrounding rock masses also used based on laboratory model test and energy analysis method by Li (2007). The criterion is expressed by the condition

$$\sigma_1 \geq \frac{K_{IC} \sqrt{\pi L}}{L(\sin \theta \cos^2 \theta - \mu \sin^2 \theta \cos \theta)} + \sigma_3 \frac{\pi + (\sin \theta \cos^2 \theta + \mu \cos^3 \theta)}{(\sin \theta \cos^2 \theta - \mu \sin^2 \theta \cos \theta)} \quad (27)$$

Where:  $\mu$  is the friction coefficient of crack surface,  $L$  is the length of the splitting crack and  $\theta$

is the angle between the original crack and the major principal stress.

It is assumed only the joint with higher dip angle will have a significant effect on producing the splitting fracture, since the joint is considered only as original crack in Eq. (27) and the major principal stress in the sidewall will be vertical. Therefore the angle  $\theta$  can be obtained as  $\theta=45.5^\circ$ . According to the field observation the length  $L$  is predicted as  $L=10$  m and  $\mu=0.5$ .

The above equation is also used to calculate the depth of the splitting damage zone based on the elastic-plastic analysis results. The calculation results using sections in Fig. 7 are shown in Fig. 9.

The damage zones obtained methods are little bit difference between Fig. 8 and Fig. 9. For some parts of rock surrounding the two research methods are verified both by borehole TV camera stated in following. From Figs. 8 and 9, the damage areas distributions calculated by the above two methods are very similar each other. But the damage zone in Figure 8 is a little bit bigger, since the numerical method based on rock bridge fracture model is used to calculate the crack evolution process gradually step by step. But the damage zone in Fig. 9 based on the semi theoretical and semi empirical results from substituting Eq. (27) to the final stress state computed for underground powerhouse cross-section. Therefore, it can be known the former method may reflect the evolution of damage area, which is increased gradually, but the latter method can not reflect the evaluation effect of damage area. Since, the damage area by former method for some parts of rock surrounding are larger than that by latter method. However, the damage zones based on the two methods are very closed to the observation by borehole TV at least at the monitoring location (see the next section).

From the Fig. 8, it can be seen that the depths of splitting damage zone calculated by the method with rock bridge fracture model in former method is approximately 14 m in the downstream sidewall of the powerhouse and 7 m in the upstream sidewall of the transformer chamber. These values show that the depth of the splitting damage zones obtained by the latter method is very close to those using the monitoring method in field.

### 3.4 Comparison to the field monitoring

In order to investigate the development and distribution of splitting crack zones in the powerhouse sidewall, two horizontal observation boreholes (42 m in length)(see Fig. 7) are drilled in the two side walls of the No. 4 bus bar tunnel through the rock pillar between the powerhouse and the transformer chamber. Another two horizontal observation boreholes are drilled below the bus bar tunnel from the powerhouse to the downstream sidewall. Borehole TV and the strain-electric-receptivity-rate technique are used for the observations. Herein, the method for monitoring splitting failure zones by borehole TV camera is given and the results discussed.

A KDVJ-400 borehole imager and a digital panoramic borehole camera are used to observe the change of the crack zones in the powerhouse downstream sidewall and the main transformer chamber upstream sidewall. When each stage of excavation is completed, the pictures are taken by borehole TV camera in every 5m distance in the drilling borehole, and the statistics number of crack with large dip angles are taken mainly in this observation segment. The observation results are shown in Fig. 10.

Fig. 10 is a plot of the number of cracks with large dip angles counted by the borehole TV. It shows that during the excavation cracks formed gradually and increased in number in the pillar. The depth of the splitting damage zone is estimated to be approximately 15 m in the downstream sidewall of the powerhouse and 7m in the upstream sidewall of the transformer chamber. These results compare well with the calculation results given by the proposed model. It can be seen from

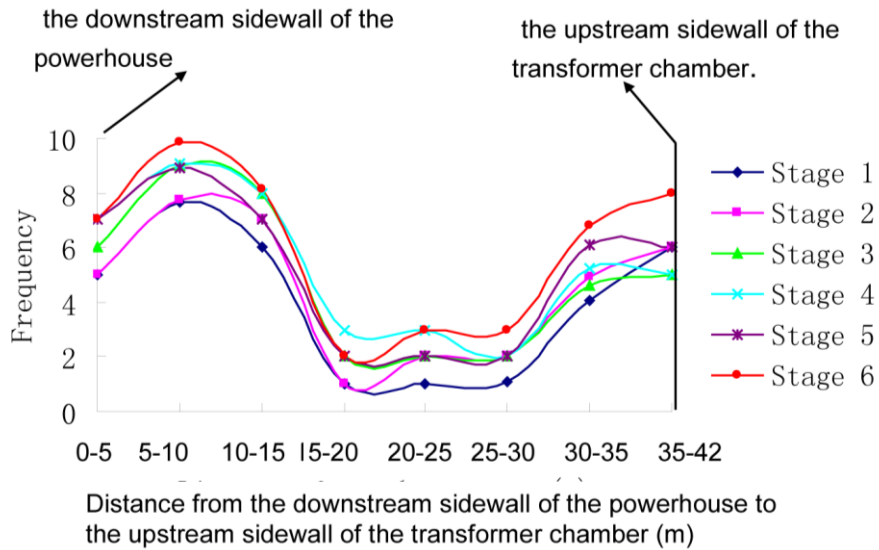


Fig. 10 Relation between the number of cracks and the borehole depth in different monitoring stages

Fig. 10, the area 14-15 m depth from the sidewall surface to the deep part of the pillar in the downstream sidewall is the cracks concentrated area (5-9 pieces larger cracks in this area in distance 5-10 m from the wall surface of power house), while the area 6-7 m depth from the sidewall surface to the deep part of the pillar in the main transformer chamber is also the cracks concentrated area (4-8 pieces larger cracks in this area for different stages). However, the central part of the rock pillar in Fig. 10, the zone from the main powerhouse wall (set to 0 in Fig. 10) to 15-30 m there are only 1-3 pieces cracks for every 5 m borehole section. Therefore, it can be consider there is 14 m splitting zone in the left of pillar center part (counting from the main transformer chamber wall), but in the right of pillar center there is 7 m vertical splitting zone (counting from main transformer chamber wall). Therefore, the damage zone depths of the observations above mentioned are very closed to the calculation results (14.7 m and 7 m) in the former part of this section. This proves that the rock bridge fracture model provided in this paper is more effective.

#### 4. Conclusions

1. The damage-fracture model and the geometric damage analysis method are adopted to investigate the effect of joints and cracks on the strength of a rock mass. A constitutive equation of the rock is established. The model considers the geometric factors associated with multiple joint sets of cracks.

2. By analyzing the formation of secondary cracks superposed on the original cracks caused by new stress condition, a damage evolution equation and failure criterion for rock bridge coalescence is established.

3. The failure criterion is applied to the numerical simulation on the rock stability of an underground engineering project, and the damage zones of rock surrounding are estimated by the

new methods. The calculated damage zones depths based on the mechanical model and splitting failure criterion are consistent with field monitoring data measured by borehole TV.

## Acknowledgments

The work is supported by the Open Research Fund of State Key Laboratory of Geomechanics and Geotechnical Engineering, Institute of Rock and Soil Mechanics, Chinese Academy of Sciences, under grant NO. Z013008, National Young Natural Science Foundation of China 41102184, National Natural Science Foundation of China 51279095. Many thanks to Prof. John Meek of Queensland University for editing this paper in English.

## References

- Barla, G, Fava, A.R. and Peri, G. (2008), "Design and construction of the Venaus powerhouse cavern in Calcschists", *Geomech. Tunnel. Bau.*, **1**, 399-406.
- Dasgupta, B., Dham, R. and Lorig, L.J. (1995), "Three dimensional discontinue analysis oft he underground powerhouse for Sardar Sarovar Project", *Proceedings of the 8<sup>th</sup> International Congress on Rock Mechanics*, Tokyo.
- Dhawan, K.R., Singh, D.N. and Gupta, I.D. (2004), "Three-dimensional finite element analysis of underground caverns", *Int. J. Geomech.*, **4**, 224-228.
- Fan, S.C., Jiao, Y.Y. and Zhao, J. (2004), "On modeling of incident boundary for wave propagation in jointed rock masses using discrete element method", *Comp. Geo. Tech.*, **31**, 57-66.
- Guo, G.X., Guo, Y.M., Qing, B.L. and Zhi, F.C. (2004), "Underground excavation in Xiaolangdi project in Yellow River", *Eng. Geol.*, **76**, 129-139.
- Hibino, S. (2003), "Rock mass and its scales", *Proceedings of 1st Kyoto International Symposium on Underground Environment*, Kyoto, Japan.
- Jiao, Y., Fan, S. and Zhao, J. (2005), "Numerical investigation of joint effect on shockwave propagation in jointed rockmasses", *J. Test. Eval.*, **33**, 197-203.
- Jiang, Y.J., Li, B. and Yamashitad, Y.J. (2009), "Simulation of cracking near a large underground cavern in a discontinuous rock mass using the expanded distinct element method", *Int. J. Rock Mech. Min. Sci. Geomech.*, **46**, 97-106.
- Kawamoto, T., Ichikawa, Y. and Kyoya, T. (1988), "Deformation and fracturing of discontinuous rock mass and damage mechanics theory", *Int. J. Numer. Anal. Meth. Geomech.*, **12**, 1-30.
- Kunin, I.A. (1983), *Elastic media with microstructure*, Springer-Verlog, Berlin, Heidelberg, New York, Tokyo.
- Li, X.J. (2007), "Research on splitting failure in deeply underground powerhouse", Shandong University Doctor's Thesis.
- Maghousa, S., Bernauda, D., Fréardb, J. and Garnierb, D. (2008). "Elastoplastic behavior of jointed rock masses as homogenized media and finite element analysis", *Int. J. Rock Mech. Min. Sci. Geomech.*, **45**, 1273-1286.
- Tezuka, M. and Seoka, T. (2003), "Latest technology of underground rock cavern excavation in Japan". *Tunnel. Underg. Space Technol.*, **18**, 127-144.
- Wang, T., Chen, X.L. and Yang, J. (2005), "Study on stability of underground cavern based on 3D GIS and 3DEC", *Chin. J. Rock Mech. Eng.*, **24**, 3476-3481.
- Wang, T., Chen, X.L. and Yu, L.H. (2005), "Discrete element calculation of surrounding rock mass stability of underground cavern group", *Rock Soil Mech.*, **26**, 1936-1940.
- Yoshida, H. and Horii, H. (2004), "Micromechanics-based continuum model for a jointed rock mass and

- excavation analyses of a large-scale cavern”, *Int. J. Rock Mech. Min. Sci.*, **41**, 119-45.
- Yoshida, H. and Horiib, H. (2003), “Micromechanics-based continuum model for a jointed rock mass and excavation analyses of a large-scale cavern”, *Int. J. Rock Mech. Min. Sci. Geomech.*, **41**, 119-145.
- Zhu, W.S., Li, X.J., Guo, Y.S., Sun, A.H. and Sui, B. (2004), “Systematical study on stability of large underground houses”, *Chin. J. Rock Mech. Eng.*, **23**, 1689-1693. (in Chinese)
- Zhu, W.S., Sun, A.H. and Sui, B. (2005), “Systematic analysis of underground cavern groups in background for Er’tan project”, *Chin. J. Underg. Space Eng.*, **1**, 15-18. (in Chinese)
- Zhu, W.S., Sui, B., Li, X.J., Li, S.C. and Wang, W.T. (2008), “A methodology for studying the high wall displacement of large scale underground cavern groups and it’s applications”, *Tunnel Underg. Space Tech.*, **6**, 651-664.